

# Dalton Transactions

Accepted Manuscript



This is an *Accepted Manuscript*, which has been through the Royal Society of Chemistry peer review process and has been accepted for publication.

*Accepted Manuscripts* are published online shortly after acceptance, before technical editing, formatting and proof reading. Using this free service, authors can make their results available to the community, in citable form, before we publish the edited article. We will replace this *Accepted Manuscript* with the edited and formatted *Advance Article* as soon as it is available.

You can find more information about *Accepted Manuscripts* in the [Information for Authors](#).

Please note that technical editing may introduce minor changes to the text and/or graphics, which may alter content. The journal's standard [Terms & Conditions](#) and the [Ethical guidelines](#) still apply. In no event shall the Royal Society of Chemistry be held responsible for any errors or omissions in this *Accepted Manuscript* or any consequences arising from the use of any information it contains.

# Synthesis and Order-Disorder Transition in Novel Metal Formate Framework of $[(\text{CH}_3)_2\text{NH}_2]\text{Na}_{0.5}\text{Fe}_{0.5}(\text{HCOO})_3$

Mirosław Mączka,<sup>\*,a</sup> Adam Pietraszko,<sup>a</sup> Lucyna Macalik,<sup>a</sup> Adam Sieradzki,<sup>b</sup> Justyna Trzmiel,<sup>b</sup> and Adam Pikul<sup>a</sup>

## ABSTRACT

We report the synthesis, crystal structure, thermal, dielectric, Raman, infrared, and magnetic properties of  $[(\text{CH}_3)_2\text{NH}_2][\text{Na}_{0.5}\text{Fe}_{0.5}(\text{HCOO})_3]$  (DMNaFe), the first metal formate framework templated by organic cations, presenting an  $\text{ABO}_3$  perovskite architecture with  $\text{NaO}_6$  octahedra as building blocks of the framework. On the basis of Raman and IR data, assignment of the observed modes to respective vibrations of atoms is proposed. We have found that DMNaFe undergoes a structural phase transition at 167 K on cooling. According to the X-ray diffraction, the compound shows  $R\bar{3}$  symmetry at 293 K, and triclinic  $P\bar{1}$  symmetry at 110 K. The  $\text{DMA}^+$  cations are dynamically disordered in the high-temperature phase and the phase transition is associated with ordering of the  $\text{DMA}^+$  cations and distortion of the metal formate framework. The dielectric studies reveal pronounced dielectric dispersion that can be attributed to slow dynamics of the  $\text{DMA}^+$  cations. Based on the low-temperature magnetic studies, this compound is weak ferromagnet with the critical temperature 8.5 K.

## Introduction

Metal-formate frameworks (MOFs) have received a great deal of attention in recent years due to their potential applications as catalysts, chemical sensors, luminescent materials.<sup>1</sup> They are also attractive materials for gas storage and some of them exhibit useful ferroelectric or even multiferroic properties.<sup>2</sup> One large family of MOFs are metal formates templated by organic cations of general formula [cat][M(HCOO<sub>3</sub>)] with M=Mg, Zn, Mn, Ni, Co, Fe, and cat = ammonium,<sup>3,4</sup> methylammonium,<sup>5</sup> dimethylammonium (DMA),<sup>5-9</sup> guanidinium,<sup>10</sup> azetidinium,<sup>11</sup> formamidinium,<sup>12</sup> etc. Most reported compounds were those templated by DMA<sup>+</sup> and NH<sub>4</sub><sup>+</sup> cations since they exhibit coexistence of electric and magnetic order at the same phase below an order-disorder phase transition temperature.<sup>3,6-9</sup> However, many attempts were also undertaken to synthesize novel compounds by changing the organic cation in hope to obtain materials with improved ferroelectric or multiferroic properties, or even novel functionality. In this respect, synthesis of azetidinium analogues led to materials with giant dielectric anomalies, whereas formamidinium compounds have significant CO<sub>2</sub> sorption capacity, which make them attractive "sponge" for gas storage applications.<sup>11,12</sup> Although using different organic cations was most extensively used in order to modify the functional properties of [cat][M(HCOO<sub>3</sub>)] compounds, a few attempts have also been undertaken to synthesize novel MOFs by modifying the metal-organic framework itself. That is, synthesis of three novel compounds containing DMA<sup>+</sup> cation and M<sup>II</sup>O<sub>6</sub> (M<sup>II</sup>=Mn, Co, Fe) and Fe<sup>III</sup>O<sub>6</sub> octahedral units have been reported, and coexistence of magnetic and antiferroelectric order was found for the mixed valence [(CH<sub>3</sub>)<sub>2</sub>NH<sub>2</sub>][Fe<sup>II</sup>Fe<sup>III</sup>(HCOO)<sub>6</sub>] formate.<sup>13</sup> It is worth noting that presence of trivalent iron in the structure is compensated by reduction in the number of DMA<sup>+</sup> cations present in the cavities of the framework.<sup>13</sup> This leads to significant change of the crystals structure, that is, whereas the

$[(\text{CH}_3)_2\text{NH}_2][\text{M}(\text{HCOO})_3]$  compounds crystallize in the perovskite-type structures,<sup>6,8,9</sup> the  $[(\text{CH}_3)_2\text{NH}_2][\text{M}^{\text{II}}\text{Fe}^{\text{III}}(\text{HCOO})_6]$  compounds possess niccolite-type structure.<sup>13</sup>

MOFs of formula  $[(\text{CH}_3)_2\text{NH}_2][\text{M}(\text{HCOO})_3]$  with  $\text{M}=\text{Mn}, \text{Zn}, \text{Ni}, \text{Co}, \text{Fe}$  crystallize in the trigonal space group  $R\bar{3}c$ , with the disordered  $\text{DMA}^+$  cations located in the cages of the network.<sup>6,8,9</sup> They exhibit electric ordering at 160-185 K, associated with ordering of the  $\text{DMA}^+$  cations and the decrease of symmetry to  $Cc$ .<sup>6,9</sup> They also show magnetic ordering at 8-36 K.<sup>8,9</sup>

Herein, we report synthesis and study of the novel  $[(\text{CH}_3)_2\text{NH}_2][\text{Na}_{0.5}\text{Fe}_{0.5}(\text{HCOO})_3]$  (DMNaFe) compound, which shows similar metal-formate framework as in  $[(\text{CH}_3)_2\text{NH}_2][\text{M}(\text{HCOO})_3]$  but with  $\text{Na}^{\text{I}}$  and  $\text{Fe}^{\text{III}}$  ions instead of  $\text{M}^{\text{II}}$  ones. This formate is characterized by single crystal X-ray diffraction (XRD), heat capacity, dielectric anomaly, measurements of low temperature magnetization, Raman scattering and IR spectroscopy. It should be emphasized that reported here synthesis of DMNaFe is a novel way of modifying the metal formate framework, not explored before. That is, we use for the first time monovalent sodium cations, which do not occupy cavities of the framework but participate in formation of the anionic framework. Using monovalent and trivalent cations, instead of divalent and trivalent cations reported previously, allows to maintain charge of the anionic framework and no reduction in the number of  $\text{DMA}^+$  counter ions is necessary, as in the case of reported  $[(\text{CH}_3)_2\text{NH}_2][\text{M}^{\text{II}}\text{Fe}^{\text{III}}(\text{HCOO})_6]$  compounds. We will show that this type of substitution preserves a perovskite-type structure but leads to significant modifications of the physicochemical properties.

## Experimental

### Materials and instrumentation

HCOONa (99%, Fluka), FeCl<sub>2</sub> (98%, Aldrich), DMA•HCl (DMA•HCl = dimethylamine hydrochloride) (99%, Aldrich) and N,N-dimethylformamide (DMF) (99.8%, Aldrich) were commercially available and used without further purification. Elemental analysis (C, H, N) was performed on a Elementar Vario EL CHNS analyzer. Na to Fe ratio in the obtained crystals was established based on EDS spectra, which were acquired and analyzed using an EDAX Pegasus XM4 spectrometer with SDD Apollo 40 detector, attached to an FEI Nova NanoSEM 230 microscope. Heat capacity was measured using Mettler Toledo DSC-1 calorimeter with high resolution of 0.4 μW. Sample weight was chosen to be 13.2 mg. Sample was slightly crushed to ensure good thermal contact. Nitrogen was used as a purging gas. Temperature change rate was chosen to be 5 K/min and the DSC thermograms were taken for both cooling and heating cycles. The excess heat capacity associated with the phase transition was calculated by subtraction from the data the baseline representing variation in the absence of the phase transitions. The dielectric measurements at ambient pressure were carried out using a Novocontrol Alpha impedance analyzer (10<sup>-2</sup>-10<sup>6</sup> Hz). Since the obtained single crystals were not big enough to perform single crystal dielectric measurements, pellets made of well-dried samples were measured instead. Using of pellet instead of a single crystal gives average response from both ε<sub>c</sub> and ε<sub>a</sub> dielectric permittivities. The pellets were placed between two copper, flat electrodes of the capacitor with a gap of 0.4 mm. The small signal of an amplitude 1V was applied across the sample. The temperature was controlled by the Novo-Control Quattro system, with use of a nitrogen gas cryostat. The measurements were taken every 1 deg over the temperature range from 140 to 260 K. Temperature stability of the samples was better than 0.1 K. Magnetic properties of a large number of freely oriented single crystals of DMNaFe (about 30 mg in total) were measured on a

commercial Quantum Design superconducting quantum interference device (SQUID) magnetometer in temperature range 2–30 K and in external magnetic fields up to 500 Oe. The residual magnetic field of the superconducting magnet used is of the order of a few Oe. The background coming from weakly diamagnetic sample holder (not shown here) was found to be negligible, thus its subtraction was omitted. Also no demagnetization corrections were made to the data reported here. Powder XRD pattern was obtained on a X'Pert PRO X-ray diffraction system equipped with a PIXcel ultrafast line detector, and Soller slits for  $\text{CuK}\alpha_1$  radiation ( $\lambda=1.54056 \text{ \AA}$ ). Single-crystal data sets of the sample were collected at 293 and 110 K on a 4-circle diffractometer KM4CCD (Oxford Diffraction) using a graphite monochromated  $\text{MoK}\alpha$  radiation ( $\lambda = 0.71073 \text{ \AA}$ ). For the low temperature measurements, the crystal temperature was maintained using an open flow nitrogen cryosystem (Oxford Cryosystem). Raman spectra were measured using a Bruker FT 100/S spectrometer with YAG:Nd laser excitation (1064 nm) and a helium-flow Oxford cryostat. Since the FT-Raman spectra were noisy, additional Raman spectra were measured using a Renishaw InVia Raman spectrometer equipped with confocal DM 2500 Leica optical microscope, a thermoelectrically cooled CCD as a detector, a diode laser operating at 830 nm and a cryostat cell THMS600 operating down to 80 K. Temperature dependent IR spectra were measured for the sample in KBr pellet in the range of  $3800\text{-}400 \text{ cm}^{-1}$  and in Apiezon N suspension in the range of  $500\text{-}50 \text{ cm}^{-1}$  with the Biorad 575C FT-IR spectrometer using a helium-flow Oxford cryostat. The resolution was  $2 \text{ cm}^{-1}$ .

### **Synthesis of the sample**

DMNaFe crystals were prepared under solvothermal conditions at  $140 \text{ }^\circ\text{C}$ . In a typical experiment, a mixture of  $\text{FeCl}_2$  (4 mmol),  $\text{HCOONa}$  (12 mmol),  $\text{DMA}\cdot\text{HCl}$  (4 mmol), DMF (30

mL), and H<sub>2</sub>O (30 mL) was heated in a Teflon-lined microwave autoclave for 48 h. Block light yellow crystals were obtained by evaporating the solution at room temperature for 20 days. The crystals were filtered from the mother liquid and washed by ethanol. The yield is about 40 % based on the starting iron salt. Anal. Calcd: C, 27.23; H, 5.03; N, 6.35. Found: C, 26.91; H, 4.29; N, 6.09. The Na:Fe ratio is 1:1 within the accuracy of the EDS spectra (see Figure S1 in the Supporting Information). A good match of its powder XRD pattern with the calculated one based on the single-crystal structure (see Figure S2) confirmed the phase purity of the bulk sample.

**Crystallographic Structure Determination.** The CrysAlis software version 1.170.33.42 was used for data processing.<sup>14</sup> An empirical absorption correction was applied using spherical harmonics implemented in SCALE3 ABSPACK scaling algorithm. The structure was solved by direct methods and refined by the full-matrix least-squares method by means of SHELX-97 program package.<sup>15</sup>

## Results and discussion

### Thermal properties

The DSC measurements show a heat anomaly at 170.8 K upon warming and 167.0 K upon cooling (Figure S3). The change in heat capacity related to the phase transition is presented in Figure 1. The shape of the curve points to a first-order transition. The associated change in enthalpy  $\Delta H$  and entropy  $\Delta S$  was estimated to be  $\sim 0.17 \text{ kJmol}^{-1}$  and  $\sim 0.9 \text{ Jmol}^{-1}\text{K}^{-1}$ , respectively. According to our X-ray diffraction studies, the DMA<sup>+</sup> cation shows trigonal disorder in the high temperature (HT) phase (see discussion in the next paragraphs of the present paper). For an order-disorder transition,  $\Delta S = R \ln(N)$ , where N is the number of sites for the disordered system. Therefore, for a simple 3-fold order-disorder model  $\Delta S$  should be  $9.1 \text{ Jmol}^{-1}$

$^1\text{K}^{-1}$ . Our data show that  $\Delta S$  is an order of magnitude smaller than the expected value. Similar behavior was previously noticed for  $[(\text{CH}_3)_2\text{NH}_2][\text{M}(\text{HCOO})_3]$  compounds with  $\text{M}=\text{Mn}$ ,  $\text{Zn}$ ,  $\text{Ni}$ ,  $\text{Mg}$  and  $\text{Fe}$ ,  $\text{Co}$ ,<sup>6,9</sup> and it indicates that that the phase transition is more complex than expected on the basis of a simple 3-fold order-disorder model.

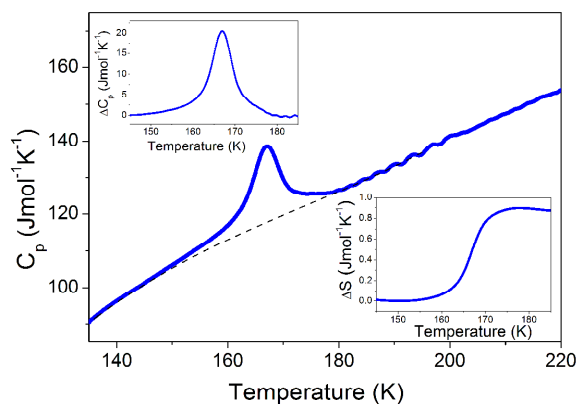


Figure 1. Heat capacity of DMNaFe measured in cooling mode. The insets show the change in  $C_p$  and  $S$  related to the phase transition.

### Dielectric Properties

Temperature dependence of imaginary (a) and real part (b) of the complex dielectric permittivity  $\varepsilon(\omega)=\varepsilon'-i\varepsilon''$  is presented in Figure 2. The real part of permittivity  $\varepsilon'$  displays a step-like increase. The imaginary part  $\varepsilon''$  exhibits a broad peak at frequencies where the  $\varepsilon'$  branch increases most steeply (Figure 2). The temperature  $T_m$  at which the maximum of the real part of dielectric permittivity occurs and the magnitude  $\varepsilon_{\max}$  of broadened  $\varepsilon'(T)$  peak are strictly frequency dependent for all frequencies available for measurements, but at temperatures slightly above  $T_m$ ,  $\varepsilon$  is practically frequency independent (see Figure 2). In both the imaginary and real part of dielectric permittivity there are no significant changes indicating a phase transition.

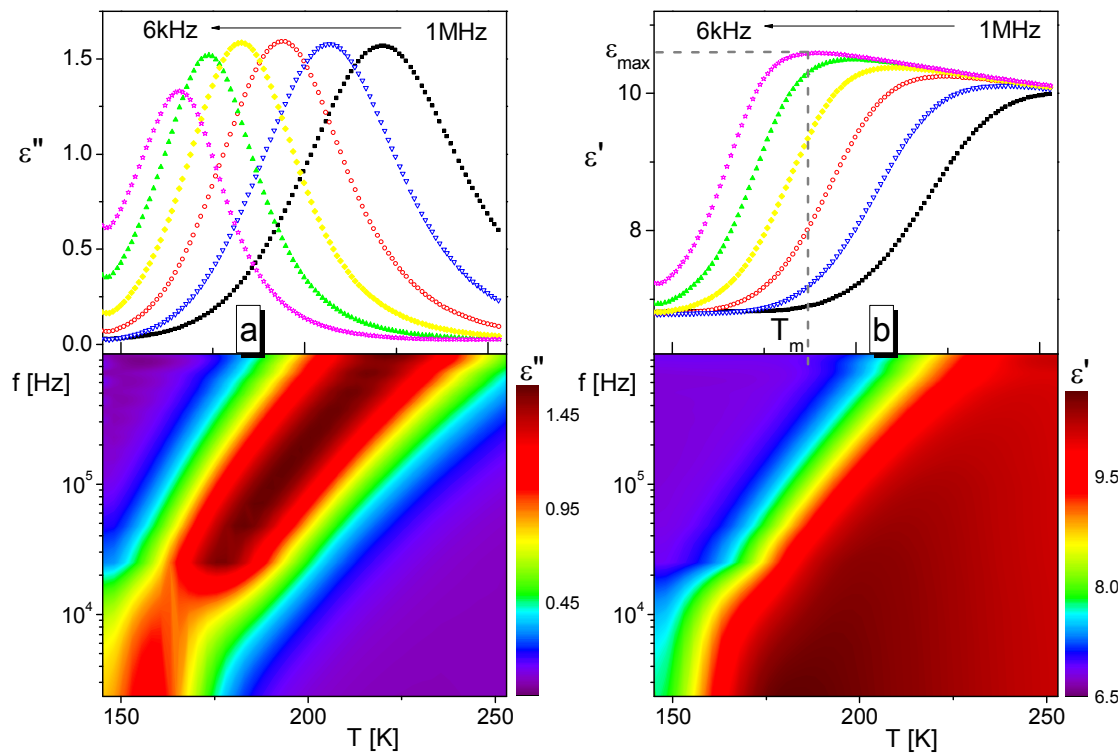


Figure 2. (a) The imaginary and (b) real part of dielectric permittivity for DMNaFe measured at different frequencies as a function of temperature.

The observed behavior is characteristic of a Debye-like dielectric relaxation and in such case the  $\epsilon'$  and  $\epsilon''$  are expressed by the following equations:

$$\epsilon'(\omega) = \frac{\epsilon_0 - \epsilon_\infty}{1 + \omega^2 \tau^2} + \epsilon_\infty \quad (1)$$

$$\epsilon''(\omega) = \frac{(\epsilon_0 - \epsilon_\infty) \omega \tau}{1 + \omega^2 \tau^2} \quad (2)$$

where  $\tau$ ,  $\omega$ ,  $\epsilon_0$  and  $\epsilon_\infty$  are the relaxation time, frequency, static dielectric constant and high-frequency dielectric constant, respectively. The Cole-Cole plots (Figure 3) exhibit semicircles for

temperatures above  $T_c$ , representing the Debye-type dielectric relaxation with a single relaxation. Below  $T_c$ , the Cole-Cole plots deviate from the circular shape, indicating that more than one Debye-type dielectric relaxation takes place in the low temperature phase. The dielectric relaxation observed above  $T_c$  obeys the Arrhenius law for the  $\tau = \omega^{-1}$  as a function of  $T$ , with  $\tau_0 = 5.2 \times 10^{-14}$  s and  $E_a/k_B = 3.3 \times 10^3$  K  $\approx$  0.28 eV (Figure S4). The  $E_a$  value is comparable to the activation energies for reorientational motion of the  $\text{DMA}^+$  cation found in other compounds containing these cations such as  $\{(\text{CH}_3)_2\text{NH}_2\}_5\text{Cd}_3\text{Cl}_{11}$  ( $E_a=0.19$  eV) or  $[(\text{CH}_3)_2\text{NH}_2][\text{Zn}(\text{HCOO})_3]$  ( $E_a=0.24$  eV).<sup>16,17</sup> This result is a strong evidence that freezing of motions of the  $\text{DMA}^+$  cations on decreasing temperature is responsible for the dielectric anomaly in  $\text{DMNaFe}$ .

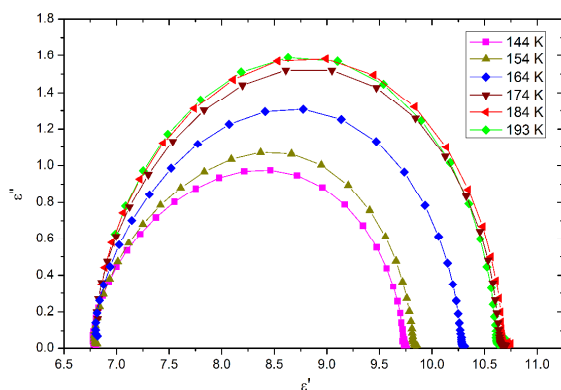


Figure 3. The Cole-Cole diagram of  $\text{DMNaFe}$  at a few temperatures.

### Magnetic Properties

Figure 4 presents temperature dependences of the magnetization  $M$  of  $\text{DMNaFe}$  measured in a nominal magnetic field of 10 Oe under zero-field-cooling (ZFC) and field-cooling (FC) conditions. As seen in the main panel, the compound exhibits a magnetic phase transition at  $T_m =$

8.5 K, the shape of which is very sensitive to the thermal history of the sample. Small hysteresis visible in the magnetization measured as a function of magnetic field (see the inset to Figure 4) indicates a ferromagnetic character of the ordering.

The behaviour observed in the studied here DMNaFe is characteristic of compounds exhibiting weak ferromagnetism, which is often caused by a small canting of the underlying antiferromagnetic lattice. Such a small canting is in general strongly sensitive on temperature, magnetic field and the strength of the coupling between the magnetic ions, and small changes in these parameters may lead to complex magnetic behavior.<sup>18</sup> Small saturation magnetization of DMNaFe, comparable to that found in other metal formates templated by dimethylammonium,<sup>8,9</sup> ammonium,<sup>3</sup> or imidazolium,<sup>19</sup> is consistent with the spin-canted mechanism of the long-range magnetic ordering in DMNaFe.

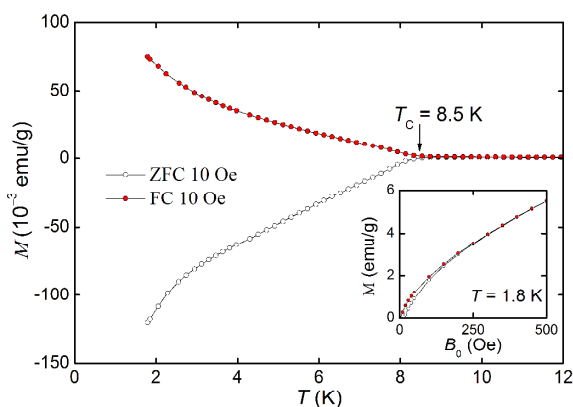


Figure 4. Temperature variation of the magnetization  $M$  of DMNaFe measured in the zero-field-cooling (ZFC) and field-cooling (FC) regimes. The negative ZFC values are most likely due to small negative residual field of zero field of the used instrument and easy magnetization of the sample. The inset: the magnetization as a function of the external magnetic field. Solid lines serve as a guide for the eye and the arrow marks the ordering temperature  $T_m$ .  $m_0H$  is the nominal magnetic field applied.

## Structural Studies

The details of data collection, data reduction, and crystallographic data obtained at 293 and 110 K are summarized in Tables S1-S3. The compound crystallizes in the trigonal system in the space group  $R\bar{3}$ . Rigid, 3D pseudo-perovskite substructure, consisting of  $\text{FeO}_6$  and  $\text{NaO}_6$  octahedra, which are connected by formate groups, accommodates  $\text{DMA}^+$  cations in the large cavities. Each iron (sodium) cation is connected to its six sodium (iron) nearest neighbors through six formate bridges in the octahedral environment, where the Fe-O and Na-O distances are 2.0121 and 2.4143 Å, respectively (see Figure S5 and Table S2). In contrast to  $[(\text{CH}_3)_2\text{NH}_2][\text{M}(\text{HCOO})_3]$  compounds, where the  $\text{HCOO}^-$  ions have  $\text{C}_2$  symmetry and equal C-O bond lengths, the formate units in  $\text{DMNaFe}$  are strongly asymmetric, with the C0-O1 and C0-O2 bonds of 1.2672 and 1.2171 Å, respectively. This difference arises from the fact that the O1 and O2 atoms connect to  $\text{Fe}^{\text{III}}$  and  $\text{Na}^{\text{I}}$  cations, respectively. The  $\text{NH}_2$  groups of  $\text{DMA}^+$  form four N-H $\cdots$ O hydrogen bonds with the anionic framework (Table 1). Two N $\cdots$ O distances, i.e. the N1 $\cdots$ O2 ones, are shorter (2.8852 and 3.0769 Å) than the corresponding distances in the  $[(\text{CH}_3)_2\text{NH}_2][\text{Mn}(\text{HCOO})_3]$  compound (2.920 and 3.2803 Å).<sup>9</sup> Moreover, the corresponding N1-H11 $\cdots$ O2 and N1-H12 $\cdots$ O2 angles are closer to 180° (174.0 and 144.0°) than N-H $\cdots$ O angles in  $[(\text{CH}_3)_2\text{NH}_2][\text{Mn}(\text{HCOO})_3]$  (159.1 and 126.5°).<sup>9</sup> This result indicates that the H-bonds formed between the  $\text{NH}_2$  groups and O2 atoms of the  $\text{NaO}_6$  octahedra are stronger than the H-bonds formed in the manganese compound. On the other hand, two remaining H-bonds in  $\text{DMNaFe}$  have significantly longer N1 $\cdots$ O1 distances (3.5321 and 3.0957 Å) and smaller N1-H11 $\cdots$ O1 and N1-H12 $\cdots$ O1 angles (126.3 and 143.7 °), indicating significantly weaker H-bond strength between the  $\text{NH}_2$  groups and O1 atoms of the  $\text{FeO}_6$  octahedra.

Despite the fact that cations interact with formate oxygen atoms via H-bonds, they are not able to overcome thermally activated motions and, as a result, rotate around three fold axis (Figure 5). Three equivalent positions of the  $\text{NH}_2$  group give six possible equivalent H-bonds, none of them is favored. The 3-fold axis passes through the two C atoms of the methyl groups and this type of disorder is very similar to that observed for other  $[(\text{CH}_3)_2\text{NH}_2][\text{M}(\text{HCOO})_3]$  compounds and  $\text{H}[\text{Mg}(\text{HCOO})_3] \supset (\text{CH}_3)_2\text{NH}$ .<sup>6,8,9,20</sup>

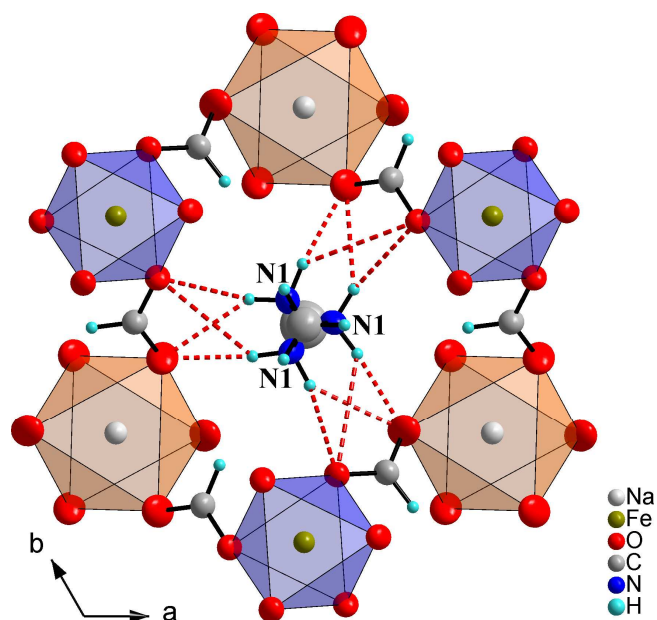


Figure 5. Distribution of disordered  $\text{DMA}^+$  cations around trigonal 3 axis in the crystal cage at 293 K. Equivalent H-bonds are shown as dashed lines.

Table 1. The geometries of the  $\text{N-H}\cdots\text{O}$  bonds between the  $\text{DMA}^+$  cations and the anionic framework at 293 K (distances, Å; angles, °).<sup>a</sup>

D-H $\cdots$ A	d(D-H)	d(H $\cdots$ A)	d(D $\cdots$ A)	$\angle(\text{DHA})$
N(1)-H(11) $\cdots$ O(1)#13	0.871	2.946	3.5321	126.3
N(1)-H(11) $\cdots$ O(2)#13	0.871	2.017	2.8852	174.0
N(1)-H(12) $\cdots$ O(1)#12	0.863	2.358	3.0957	143.7

N(1)-H(12)···O(2)#12      0.863      2.336      3.0769      144.0

<sup>a</sup>Symmetry transformations used to generate equivalent atoms: #12  $-x+y+2/3, -x+1/3, z+1/3$  #13  $-y+2/3, x-y+1/3, z+1/3$

Upon cooling, the crystal structure deformation occurs near 167 K. Observation under a polarizing microscope reveals formation of clear ferroelastic domains (see Figure S6), pointing to decrease of the symmetry to monoclinic or triclinic. The low temperature structure could be solved in the  $P\bar{1}$  space group with the cell parameters of  $a = 8.2617$ ,  $b = 9.0797$ ,  $c = 12.293$  Å,  $\alpha = 95.37$ ,  $\beta = 90.43$ , and  $\gamma = 89.91^\circ$  (see Table S1). At 110 K, the DMA<sup>+</sup> cations are ordered (see Figure S7). Table S2 shows that there are two unique DMA<sup>+</sup> cations. Both of them form H-bonds to the anionic framework (see Table S3). Similarly as in the room temperature phase, stronger H-bonds are formed between the NH<sub>2</sub> groups and NaO<sub>6</sub> octahedra. Interestingly, the H-bond strength is significantly different for the both unique DMA<sup>+</sup> cations. For the first DMA<sup>+</sup> cation, the N···O distances (O corresponds to NaO<sub>6</sub> octahedra) are 2.977 and 3.104 Å, whereas for the second DMA<sup>+</sup> the corresponding distances are 2.896 and 2.998 Å (see Table S3). Another interesting feature of the low temperature structure is distortion of the anionic framework: i) all Na<sup>I</sup> and Fe<sup>III</sup> cations are in distorted octahedral environments, with six different Na-O and Fe-O distances (Table S2), ii) the number of unique HCOO<sup>-</sup> ions increases from one in the room temperature structure to six at 110 K.

The evolution of the lattice parameters as a function of temperature shows that the lattice parameters exhibit very clear anomalies near  $T_c$  (Figure 6). Discontinuous changes of the parameters  $a$  and  $c$  point to a first order nature of the phase transition in DMNaFe. It is worth noting that the parameter  $b$  expands upon cooling in the low temperature phase. Thus the low temperature phase of DMNaFe exhibits negative thermal expansion (NTE) in the  $b$ -direction.

NTE properties have previously been reported for  $[\text{NH}_4][\text{Mg}(\text{HCOO})_3]$ , possessing chiral framework of  $4^9 \cdot 6^6$  topology,<sup>4,21</sup> and disordered structures of perovskite  $[\text{CH}_3\text{CH}_2\text{NH}_3][\text{Mg}(\text{HCOO})_3]$  and niccolite  $[\text{NH}_3(\text{CH}_2)_4\text{NH}_3][\text{Mg}(\text{HCOO})_3]$  above 363 and 390 K, respectively.<sup>21</sup> But it has not yet been reported for ordered metal formates templated by organic cation possessing perovskites architecture of  $4^{12} \cdot 6^3$  topology. In particular, recent temperature-dependent studies of  $[(\text{CH}_3)_2\text{NH}_2][\text{Mn}(\text{HCOO})_3]$  showed usual contraction of all lattice parameters upon cooling both in the high and low temperatures phases.<sup>22</sup>

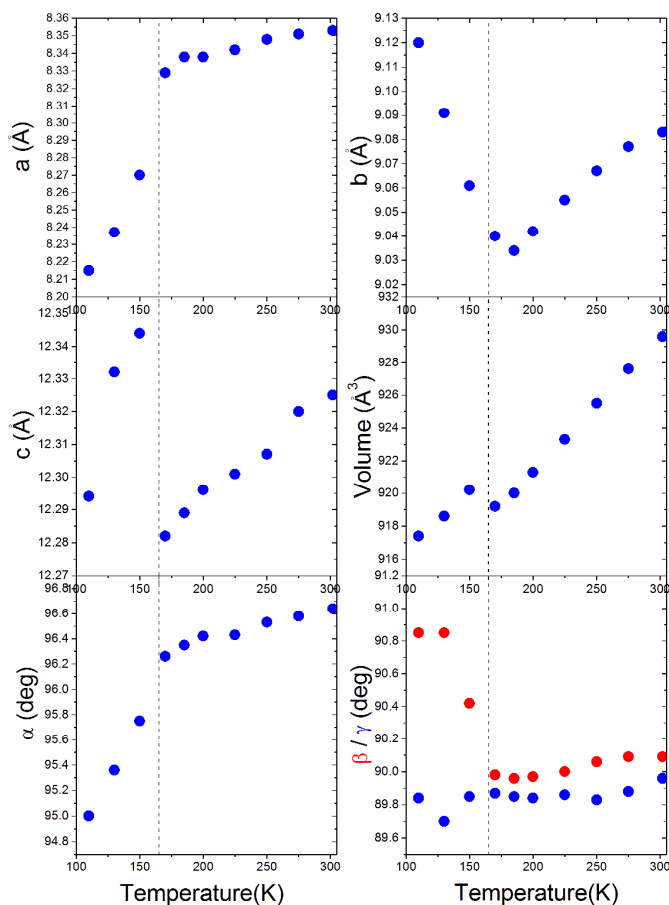


Figure 6. Temperature dependence of DMNaFe lattice parameters for the LT and HT phases. The parameters of the HT phase were recalculated in the triclinic system to facilitate the comparison.

The transformation matrix is as follow:

$$\begin{pmatrix} -1 & 0 & 0 \\ 0.3333 & 0.6667 & 0.3333 \\ -0.6667 & -1.3333 & 0.3333 \end{pmatrix}$$

Experimental data are shown as circles. The vertical lines indicate the temperature at which DMNaFe undergoes the phase transition.

### Vibrational Studies

The Raman and IR spectra of DMNaFe are presented in Figures 7, 8 and S8-S11, Supporting Information. The observed IR and Raman frequencies (in  $\text{cm}^{-1}$ ) are listed in Table S4, Supporting Information together with suggested assignments that were mostly based on literature data.<sup>4,9,23-25</sup>

It is worth comparing the spectra of DMNaFe with the spectra of previously studied  $[(\text{CH}_3)_2\text{NH}_2][\text{M}(\text{HCOO})_3]$  compounds with  $\text{M}=\text{Fe}, \text{Mn}, \text{Ni}, \text{Zn}$ .<sup>9,25</sup> The comparison shows that the bands related to vibrations of the  $\text{CH}_3$  and  $\text{CNC}$  groups are observed at similar frequencies in DMNaFe and  $[(\text{CH}_3)_2\text{NH}_2][\text{M}(\text{HCOO})_3]$  compounds. However, the  $\nu(\text{NH}_2)$  and  $\rho(\text{NH}_2)$  modes of DMNaFe are observed at slightly higher and lower frequencies, respectively, when compared to  $[(\text{CH}_3)_2\text{NH}_2][\text{M}(\text{HCOO})_3]$  compounds. DFT calculations of vibrational properties of  $[(\text{CH}_3)_2\text{NH}_2][\text{Ni}(\text{HCOO})_3]$  showed that these modes are very sensitive on the formation of H-bonds, that is, when H-bonds are formed the  $\nu(\text{NH}_2)$  and  $\rho(\text{NH}_2)$  modes shift to lower and higher frequencies, respectively.<sup>25</sup> Thus our IR data suggest that the H-bond strength is slightly weaker in DMNaFe when compared to  $[(\text{CH}_3)_2\text{NH}_2][\text{M}(\text{HCOO})_3]$  compounds. In contrast to vibrations of the  $\text{DMA}^+$  cations, which exhibit relatively weak changes when going from

$[(\text{CH}_3)_2\text{NH}_2][\text{M}(\text{HCOO})_3]$  to  $\text{DMNaFe}$ , vibrations of the formate groups exhibit very pronounced changes. In particular, the  $\nu_2$  modes of  $\text{DMNaFe}$  shift by  $70\text{-}80\text{ cm}^{-1}$  toward lower frequencies, when compared to the corresponding modes of  $[(\text{CH}_3)_2\text{NH}_2][\text{M}(\text{HCOO})_3]$ . Moreover, the  $\nu_4$  mode of  $[(\text{CH}_3)_2\text{NH}_2][\text{M}(\text{HCOO})_3]$  at  $1587\text{-}1594\text{ cm}^{-1}$  splits into two components in  $\text{DMNaFe}$  at  $1595$  and  $1632\text{ cm}^{-1}$ . These features reflect a significant difference in the C-O bond lengths of the formate groups in  $\text{DMNaFe}$ .

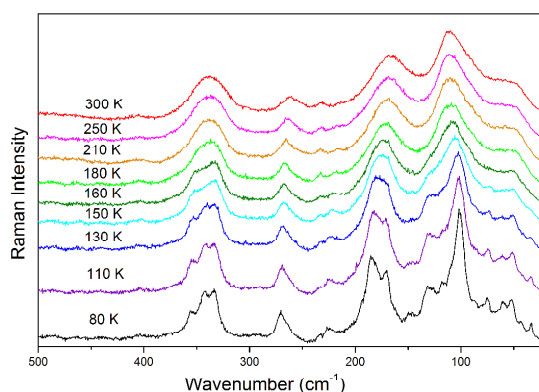


Figure 7. Raman spectra in the spectral range  $25\text{-}500\text{ cm}^{-1}$ . The spectra were normalized by the Bose-Einstein factor, i.e., the experimental spectra were divided by  $n(\omega)+1$ , where  $n(\omega) = 1/[\exp(\hbar\omega/k_B T)-1]$  is the Bose-Einstein factor.

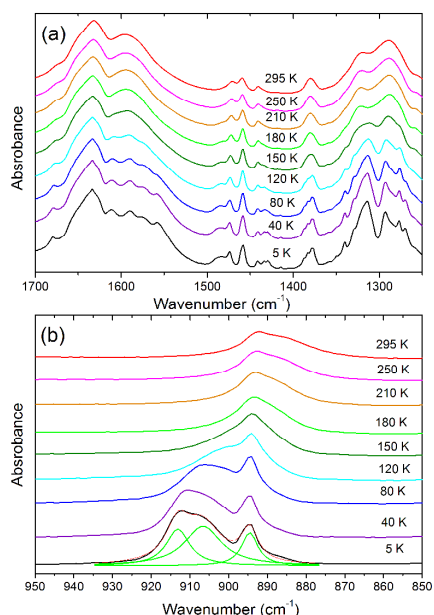


Figure 8. Detail of the IR spectra results corresponding to the spectral ranges 1250-1700, and 850-950  $\text{cm}^{-1}$ . The green plots in (b) show deconvolution of the spectrum measured at 5 K into Lorentzian components.

### Temperature-dependent Raman and IR Studies

Decreasing of temperature leads to significant changes in intensity, full width at half maximum (FWHM) and frequency of the bands related to vibrations of the  $\text{NH}_2$  groups. First, the  $\nu(\text{NH}_2)$  and  $\rho(\text{NH}_2)$  modes exhibit softening and hardening, respectively, with a decrease in temperature (Figures 8b and S10, Table S4). This behavior indicates an increase of the H-bond strength with decreasing temperature. Second, FWHM values of the IR bands attributed to the  $\nu(\text{NH}_2)$  and  $\rho(\text{NH}_2)$  vibrations decrease upon cooling. Third, the bands near 1480 and 1430  $\text{cm}^{-1}$ , attributed to  $\omega(\text{NH}_2)$  and  $\tau(\text{NH}_2)$  modes, respectively, are hardly visible at room temperature but their intensity strongly increases below 180 K (Figure 8a). The observed changes in FWHM and

intensity of the discussed bands reflect the highly dynamic nature of H-bonds in the high-temperature phase of DMNaFe and provides evidence for proton ordering in the N-H $\cdots$ O bonds at low temperatures. It is worth noting that at low temperatures the  $\rho(\text{NH}_2)$  band clearly splits into two components at 907 and 913  $\text{cm}^{-1}$  (at 5 K, Figure 8b). This behavior proves the presence of two crystallographically distinct  $\text{DMA}^+$  cations in the low temperature phase of DMNaFe, in agreement with the discussed above x-ray diffraction data.

Figure 9a shows that the  $\nu_{\text{as}}(\text{CNC})$  mode exhibits clear change in slope of frequency vs. temperature plot near  $T_c$  (see Figure 9a). It also exhibits pronounced decrease in FWHM below  $T_c$  (Figure 9b). This behavior provides further evidence that the phase transition in DMNaFe has an order-disorder character and is primarily governed by dynamics of the  $\text{DMA}^+$  cations. Very pronounced narrowing of the lattice modes upon cooling (see Figure 7 and S11), which are very sensitive to a long-range order, is also consistent with an order-disorder character of the phase transition in DMNaFe.

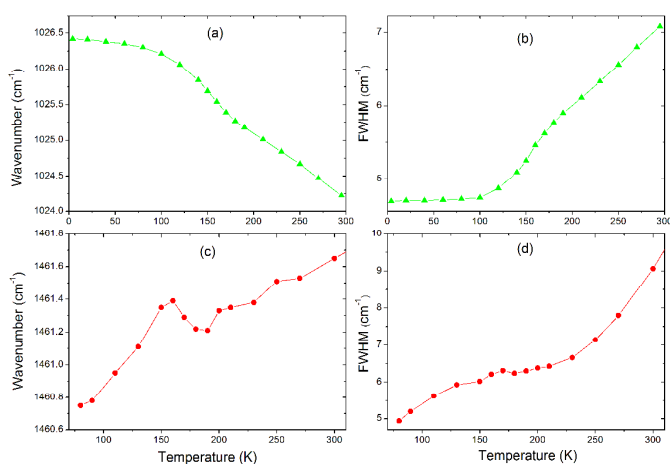


Figure 9. Temperature evolution of  $\nu_{\text{as}}(\text{CNC})$  mode IR frequencies (a) and FWHM (b). Plots (c) and (d) present temperature evolution of  $\delta_{\text{as}}(\text{CH}_3)$  mode Raman frequencies and FWHM, respectively. Solid lines are to guide the eye.

Figures 9c and 9d as well as Table S4 show that the  $\delta_{\text{as}}(\text{CH}_3)$  mode at  $1462\text{ cm}^{-1}$ ,  $\nu_{\text{as}}(\text{CH}_3)$  mode at  $3032\text{ cm}^{-1}$  and the  $\nu_{\text{s}}(\text{CH}_3)$  mode at  $2975\text{ cm}^{-1}$  soften upon cooling. The observed softening of the  $\text{CH}_3$  stretching and bending modes suggests decrease of the C-H bond lengths upon cooling.

The  $1679$  and  $1342\text{ cm}^{-1}$  Raman-active modes of formate ions also exhibit clear change of slope near  $T_c$  for frequency vs temperature plots (see Figure S12). The corresponding FWHM values exhibit weak changes down to  $T_c$  followed by fast decrease below  $T_c$ . Another characteristic feature is splitting of the broad Raman bands at  $1318$  and  $1283\text{ cm}^{-1}$ , attributed to the  $\nu_2(\text{HCOO}^-)$  mode, into doublets below  $T_c$  (see Figures S9 and S13a). This splitting is large, up to  $12\text{ cm}^{-1}$  for the lower frequency band. Significant splitting below  $T_c$  is also observed for the  $\nu_4(\text{HCOO}^-)$  mode (see Figure 8 and Table S4). This behavior indicates that the phase transition is associated with a decrease of symmetry and significant distortion of the metal-formate framework, that is, further increase of the difference in the C-O bond lengths of the formate groups in the low temperature phase. Lowering of symmetry is also evidenced by pronounced splitting of many lattice modes (see Figures 7, S11 and S13b).

### **Mechanism of the phase transition and structural relevance of the polar order in perovskite like metal formates templated by organic cations**

The obtained data show that the phase transition in  $\text{DMNaFe}$  has a first order character. X-ray diffraction data show that upon cooling,  $a_{\text{tric}}$  shrinks by about 0.7% whereas  $c_{\text{tric}}$  and  $b_{\text{tric}}$  expands by about 0.2 and 0.5 %, respectively. Interestingly, the unit cell volume also expands by about 0.1%. This behavior is significantly different from that reported for  $[(\text{CH}_3)_2\text{NH}_2][\text{Mn}(\text{HCOO})_3]$ ,

for which all parameters experienced decrease at  $T_c$ , up to 1.1 %, and volume decreased by about 0.2 %.<sup>22</sup> As can be noticed, the overall changes of the lattice parameters and volume at  $T_c$  are more pronounced for  $[(CH_3)_2NH_2][Mn(HCOO)_3]$ . Smaller structural distortion at  $T_c$  in DMNaFe is consistent with the observed by us weaker changes in vibrational frequencies and FWHM values in DMNaFe, when compared to  $[(CH_3)_2NH_2][M(HCOO)_3]$  with  $M=Mn, Ni, Zn, Fe$ .<sup>4,25</sup> Another significant difference between DMNaFe and  $[(CH_3)_2NH_2][M(HCOO)_3]$  compounds is that the low temperature phase of DMNaFe contains two unique  $DMA^+$  cations, in contrast to only one unique  $DMA^+$  in the latter case.<sup>9</sup> Furthermore, the number of unique formate ions (6) is doubled in DMNaFe, when compared to  $[(CH_3)_2NH_2][M(HCOO)_3]$ .<sup>9</sup>

In spite of these differences, DMNaFe and  $[(CH_3)_2NH_2][M(HCOO)_3]$  compounds share also common features: i) the low temperatures phases show all different Mn-O (Fe-O and Na-O) bonds, ii) the driving force for the phase transitions in both DMNaFe and  $[(CH_3)_2NH_2][M(HCOO)_3]$  compounds seem to be mainly the cooperative freezing of the molecular rotation of the  $DMA^+$  cations via hydrogen bonding rather than tilting of the  $MO_6$  octahedra and displacement of the  $DMA^+$  cations. This cooperative freezing was shown to be responsible for onset of a long-range polarization order in  $[(CH_3)_2NH_2][M(HCOO)_3]$ . However, it has recently been proposed for  $[(CH_3)_2NH_2][Mn(HCOO)_3]$  that presence of a flexible anionic framework is also the basic “ingredient” for the appearance of sharp dielectric phase transition.<sup>22</sup> Thus the authors stated that it is still not clear what mechanism is initially responsible for the transition.<sup>22</sup> Here it is interesting to note that order-disorder phase transitions in the family of perovskite-type MOFs of formula  $[cat][M(HCOO)_3]$ , where cat denote an organic cation, were reported for  $cat= DMA^+, azetidinium, formamidinium, imidazolium, hydrazinium, ethylammonium$ .<sup>6,7,9,11,12,19,21,26</sup> For the manganese analogues, the phase transition temperature upon cooling was the lowest for  $DMA^+$  (181 K) and the highest for imidazolium (435 K),<sup>9,19</sup> and

it clearly increased with strength of the H-bonds formed between organic cation and the framework. This comparison confirms that cooperative freezing of the molecular rotation of the ammonium cations plays a major role in the mechanism of the phase transitions in this family of compounds.

Recent theoretical considerations showed that in  $[\text{cat}][\text{M}(\text{HCOO})_3]$  compounds, where  $\text{cat} = \text{DMA}^+$ , guanidinium, ethylammonium etc., the organic ion is the main source of polarization and the net ferroelectric polarization is due to the relative canting of the molecular dipole moments with respect to the anionic framework.<sup>27</sup> However, significant contribution comes also from the  $\text{HCOO}^-$  ligands and the induced polar distortions are derived from the  $\text{HCOO}^-$  ions due to the coupling via H-bonds.<sup>27</sup> Thus it was concluded that it is possible to tune the ferroelectric polarization by changing the magnitude and canting of the organic molecular dipole.<sup>27</sup> From these considerations it is clear that relative canting of the organic molecular dipole with respect to the framework and thus electric polarization is expected to be very sensitive on subtle structural changes. In particular, changes in the H-bond network and strength should significantly change the magnitude of net electric polarization in  $[\text{cat}][\text{M}(\text{HCOO})_3]$  and may even result in centrosymmetric crystal structures. Literature data confirm this conclusion since they showed that in the family of  $[\text{cat}][\text{M}(\text{HCOO})_3]$  compounds crystallizing in the perovskite-type structures, ferroelectric properties were so far reported only for  $\text{DMA}^+$  analogues.<sup>6</sup> Noncentrosymmetric structures at low temperatures were also reported for guanidinium (with Cu), azetidinium (with Zn), ethylammonium and hydrazinium analogues,<sup>5,11,21,26,28</sup> and among these compounds ferroelectric properties were predicted theoretically for guanidinium with Cr and Cu, and ethylammonium with Mn.<sup>10,27</sup> However, for many other analogues containing azetidinium (except Zn), formamidinium, and imidazolium, in spite of the fact that these organic cations carry an intrinsic dipole moment and order at low temperatures, the low temperature structures are

centrosymmetric. For instance, studies of  $[\text{NH}_2\text{-CH-NH}_2][\text{Mn}(\text{HCOO})_3]$  revealed that although this compound exhibits very similar order-disorder phase transition as the related  $[(\text{CH}_3)_2\text{NH}_2][\text{M}(\text{HCOO})_3]$  compounds, the  $\text{NH}_2\text{-CH}^+\text{-NH}_2$  cation does not exhibit any canting due to the presence of extensive H-bonds, and the low temperature structure shows no net polarization.<sup>12</sup> The studied here DMNaFe also crystallizes in the centrosymmetric structure although  $[(\text{CH}_3)_2\text{NH}_2][\text{Mn}(\text{HCOO})_3]$  compounds exhibit ferroelectric properties. This behavior can be attributed to change in the H-bond network when  $\text{Mn}^{\text{II}}$  ions are substituted by  $\text{Na}^{\text{I}}$  and  $\text{Fe}^{\text{III}}$  ions. In particular, our data revealed that the H-bond network becomes strongly asymmetric in DMNaFe, that is, H-bonds are formed between the  $\text{NH}_2$  groups and the  $\text{NaO}_6$  as well  $\text{FeO}_6$  octahedra but the former ones are significantly stronger.

## Conclusions

We have synthesized novel dimethylammonium metal formate with heterovalent metal ions  $\text{Na}^{\text{I}}$  and  $\text{Fe}^{\text{III}}$ . This compound can be regarded as obtained from the known  $[(\text{CH}_3)_2\text{NH}_2][\text{M}(\text{HCOO})_3]$  multiferroics ( $\text{M}$  = divalent cation) by replacing  $\text{M}^{\text{II}}$  ions by  $\text{Na}^{\text{I}}$  and  $\text{Fe}^{\text{III}}$ . DSC data revealed onset of a structural phase transition around 167 K on cooling. Our studies indicate that the process responsible for the observed dielectric anomaly is freezing of motions of  $\text{DMA}^+$  cations on decreasing the temperature. X-ray diffraction, Raman scattering and IR data support this conclusion and show that although the ferroelectric phase transition is mainly driven by ordering of  $\text{DMA}^+$  cations, it is also accompanied by significant distortion of the metal-formate framework and decrease of symmetry to triclinic. It is interesting to notice that the phase transition mechanism in DMNaFe and temperature dependence of vibrational modes show remarkable similarities to the behavior of  $[(\text{CH}_3)_2\text{NH}_2][\text{M}(\text{HCOO})_3]$  compounds. However, the

temperature evolution of structural changes and vibrational modes is less pronounced in DMNaFe, the number of nonequivalent DMA<sup>+</sup> and HCOO<sup>-</sup> ions is doubled and the low temperature structure is centrosymmetric.

Present results show a new route for tailoring properties of metal formate frameworks templated by organic cations by exploring both NaO<sub>6</sub> and M<sup>III</sup>O<sub>6</sub> building blocks in formation of the framework. This type of network is different from the reported one built up of M<sup>II</sup>O<sub>6</sub> and M<sup>III</sup>O<sub>6</sub> octahedra, which presented niccolite type centrosymmetric structure.<sup>13</sup> In particular, the employment of NaO<sub>6</sub> and Fe<sup>III</sup>O<sub>6</sub> as the building blocks preserves a perovskite topology, while leading to decrease of symmetry from  $R\bar{3}c$  to  $R\bar{3}$ . Thus it would be of great interest to explore possibility to synthesize novel metal formate frameworks containing NaO<sub>6</sub> and Fe<sup>III</sup>O<sub>6</sub> octahedra templated by other organic cations such as methylammonium, guanidinium etc., as well as metal formate frameworks containing NaO<sub>6</sub> and M<sup>III</sup>O<sub>6</sub> octahedra, where M<sup>III</sup> ≠ Fe. Especially attractive seems to be Cr<sup>III</sup> cations, since using these cations may lead to synthesis of a new class of luminescent MOFs.

### Acknowledgements

This research was supported by the National Center for Science (NCN) in Poland under project No. DEC-2011/03/B/ST5/01019.

### Notes

<sup>a</sup>Institute of Low Temperature and Structure Research, Polish Academy of Sciences, Box 1410, 50-950 Wrocław 2, Poland; [m.maczka@int.pan.wroc.pl](mailto:m.maczka@int.pan.wroc.pl); phone: +48-713954161; fax: +48-713441029

<sup>b</sup>Institute of Physics, Wrocław University of Technology, Wybrzeże Wyspiańskiego 27, 50-370

Wrocław, Poland

Electronic Supplementary Information (ESI) available: X-ray crystallographic information files (CIF) for crystal structures of DMNaFe at 293 and 110 K. Figures S1-S13: SEM images and EDS spectra, Powder X-ray diffraction, DSC traces, GML and HN fitting parameters, view of the crystal structures, domain pattern, IR and Raman spectra, temperature dependence of bandwidths and frequencies. Tables S1-S4: X-ray data collection and refinement parameters, structural parameters, and Raman and IR frequencies.

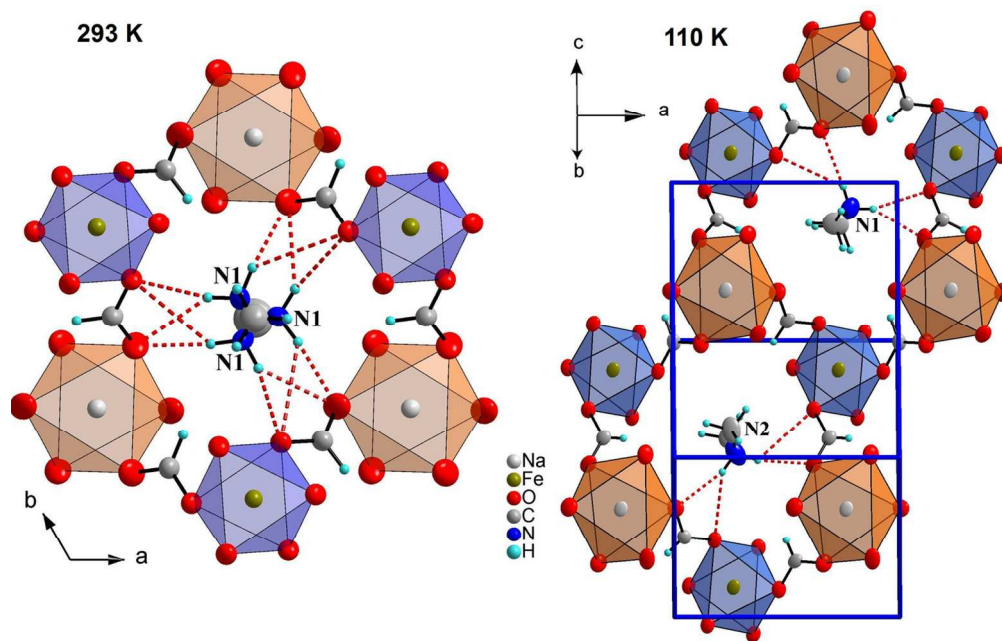
## References

- 1 (a) J. Y. Lee, O. K. Farha, J. Roberts, K. A. Scheidt, S. B. T. Nguyen and J. T. Hupp, *Chem. Soc. Rev.*, 2009, **38**, 1450; (b) L. E. Kreno, K. Leong, O. K. Farha, M. Allendorf, R. P. V. Duyne and J. T. Hupp, *Chem. Rev.*, 2012, **112**, 1105; (c) M. Allendorf, C. A. Bauer, R. K. Bhakta, R. J. T. Houk, *Chem. Soc. Rev.*, 2009, **38**, 1330.
- 2 (a) J. A. Mason, M. Veenstra and, J. R. Long, *Chem. Sci.*, 2014, **5**, 32; (b) W. Zhang and R. G. Xiong, *Chem. Rev.*, 2012, **112**, 1163; (c) G. Rogez, N. Viart and M. Drillon, *Angew. Chem. Int. Ed.*, 2010, **49**, 1921.
- 3 G. C. Xu, W. Zhang, X. M. Ma, Y. H. Hen, L. Zhang, H. L. Cai, Z. M. Wang, R. G. Xiong and S. Gao, *J. Am. Chem. Soc.*, 2011, **133**, 14948.
- 4 M. Mączka, A. Pietraszko, B. Macalik and K. Hermanowicz, *Inorg. Chem.*, 2014, **53**, 787.
- 5 Z. Wang, B. Zhang, T. Otsuka, K. Inoue, H. Kobayashi and M. Kurmoo, *Dalton Trans.*, 2004, 2209.
- 6 (a) P. Jain, V. Ramachandran, R. J. Clark, H. D. Zhou, B. H. Toby, N. S. Dalal, H. W. Kroto and A. K. Cheetham, *J. Am. Chem. Soc.*, 2009, **131**, 13625; (b) M. Guo, H. L. Cai and R. G.

- Xiong, *Inorg. Chem. Commun.*, 2010, **13**, 1590; (c) D. W. Fu, W. Zhang, H. L. Cai, Y. Zhang, J. Z. Ge, R. G. Xiong, S. D. Huang and T. Nakamura, *Angew. Chem. Int. Ed.*, 2011, **50**, 11947.
- 7 W. Wang, L.-Q. Yan, J.-Z. Cong, Y.-L. Zhao, F. Wang, S.-P. Shen, T. Zhou, D. Zhang, S.-G. Wang, X.-F. Han and Y. Sun, *Sci. Rep.*, 2013, **3**, 2024.
- 8 (a) X. Y. Wang, L. Gan, S. W. Zhang and S. Gao, *Inorg. Chem.*, 2004, **43**, 4615; (b) P. Jain, N. S. Dalal, B. H. Toby, H. W. Kroto and A. K. Cheetham, *J. Am. Chem. Soc.*, 2008, **130**, 10450.
- 9 (a) M. Maćzka, A. Gağor, B. Macalik, A. Pikul, M. Ptak and J. Hanuza, *Inorg. Chem.*, 2014, **53**, 457; (b) M. Sánchez-Andújar, S. Presedo, S. Yáñez-Vilar, S. Castro-García, J. Shamir and M. A. Señaris-Rodríguez, *Inorg. Chem.*, 2010, **49**, 1510.
- 10 (a) A. Stroppa, P. Jain, P. Barone, M. Marsman, J. M. Perez-Mato, A. K. Cheetham, H. W. Kroto and S. Picozzi, *Angew. Chem. Int. Ed.*, 2011, **50**, 5847; (b) A. Stroppa, *J. Phys. Conf. Ser.*, 2013, **428**, 012029; (c) A. Stroppa, P. Barone, P. Jain, J. M. Perez-Mato and S. Picozzi, *Adv. Mater.*, 2013, **25**, 2284.
- 11 (a) B. Zhou, Y. Imai, A. Kobayashi, Z. M. Wang and H. Kobayashi, *Angew. Chem. Int. Ed.*, 2011, **50**, 11441; (b) Y. Imai, B. Zhou, Y. Ito, H. Fijimori, A. Kobayashi, Z. M. Wang and H. Kobayashi, *Chem. Asian J.*, 2012, **7**, 2786; (c) W. Li, Z. Zhang, E. G. Bithell, A. S. Batsanov, P. T. Barton, P. J. Saines, P. Jain, C. J. Howard, M. A. Carpeneter and A. K. Cheetham, *Acta Mater.*, 2013, **61**, 4928.
- 12 (a) R. E. Marsh, *Acta Crystallogr. C*, 1986, **42**, 1327; (b) A. Rossin, M. R. Chierotti, G. Giambastiani, R. Gobetto and M. Peruzzini, *Cryst. Eng. Comm.*, 2012, **14**, 4454; (c) M. Maćzka, A. Ciupa, A. Gağor, A. Sieradzki, A. Pikul, B. Macalik and M. Drozd, *Inorg. Chem.*, 2014, **53**, 5260.
- 13 (a) K. S. Hagen, S. G. Naik, B. H. Huynh, A. Masello and G. Christou, *J. Am. Chem. Soc.*, 2009, **131**, 7516; (b) J. P. Zhao, B. W. Hu, F. Lloret, J. Tao, Q. Yang, X. F. Zhang and X. H. Bu,

- Inorg. Chem.*, 2010, **49**, 10390; (c) L. Cañadillas-Delgado, O. Fabelo, J. A. Rodríguez-Velamazán, M. H. Lemée Cailleau, S. A. Mason, E. Pardo, F. Lloret, J. P. Zhao, X. H. Bu, V. Simonet, C. V. Colin and J. Rodríguez-Carvajal, *J. Am. Chem. Soc.*, 2012, **134**, 19772.
- 14 Agilent Technology Poland, CrysAlis RED, Data Reduction Program, Issue 171.33.42.
- 15 G. M. Sheldrick, *Acta Cryst. A*, 2008, **64**, 112.
- 16 R. Sobiestianskas, K. Abe and T. Shigenari, *J. Phys. Soc. Jpn.*, 1996, **65**, 3146.
- 17 T. Asaji and K. Ashitomi, *J. Phys. Chem. C*, 2013, **117**, 10185.
- (18) (a) H. Kageyama, D. I. Khomskii, R. Z. Levitin, M. M. Markina, T. Okuyama, T. Uchimoto and A. N. Vasil'ev, *J. Magn. Magn. Mater.*, 2003, **262**, 445; (b) J. Mao, Y. Sui, X. Zhang, Y. Su, X. Wang, Z. Liu, Y. Wang, R. Zhu, Y. Wang, W. Liu and J. Tang, *Appl. Phys. Lett.*, 2011, **98**, 192510; (c) N. Dasari, P. Mandal, A. Sundaresan and N. S. Vidhyadhiraja, *Europhys. Lett.*, 2012, **99**, 17008.
- 19 P. Pato-Dolán, L. C. Gómez-Aguirre, J. M. Bermúdez-García, M. Sánchez-Andújar, A. Fondado, J. Mira, S. Castro-García and M. A. Señarís-Rodríguez, *RSC Adv.*, 2013, **3**, 22404.
- 20 A. Rossin, A. Ienco, F. Constantino, T. Montini, B. Di Credico, M. Caporali, L. Gonsalvi, P. Fornansiero and M. Peruzzini, *Cryst. Growth Design.*, 2008, **8**, 3302.
- 21 R. Zhang, G. C. Xu, Z. M. Wang and S. Gao, *Chem. Eur. J.*, 2013, **20**, 1146.
- 22 M. Sánchez-Andújar, L. C. Gómez-Aguirre, P. Pato-Dolán, S. Yáñez-Vilar, R. Artiaga, A. L. Llamaz-Saiz, R. S. Manna, F. Schnelle, M. Lang, F. Ritter, A. A. Haghghirad and M. A. Señarís-Rodríguez, *Cryst. Eng. Comm.*, 2014, **16**, 3558.
- 23 (a) M. Maćzka, J. Hanuza and A. A. Kaminskii, *J. Raman Spectrosc.*, 2006, **37**, 1257; (b) A. L. Magalhaes, S. R. R. S. Madail and M. Ramos, *J. Theor. Chem. Acc.*, 2000, **105**, 68.

- 24 (a) M. A. Moreno, O. Galvez, B. Mate, V. J. Herrero and R. Escibano, *J. Phys. Chem. A*, 2011, **115**, 70; (b) J. Su, Y. Wang, W. Li, S. Yang, G. Li, F. Liao and J. Lin, *J. Mol. Str.*, 2009, **937**, 39.
- 25 (a) M. Mączka, M. Ptak and L. Macalik, *Vib. Spectrosc.*, 2014, **71**, 98; (b) M. Mączka, W. Zierkiewicz, D. Michalska and J. Hanuza, *Spectrochim. Acta A*, 2014, **128**, 674.
- 26 S. Chen, R. Shang, K. L. Hu, Z. M. Wang and S. Gao, *Inorg. Chem. Front.*, 2014, **1**, 83.
- 27 D. Di Sante, A. Stroppa, P. Jain and S. Picozzi, *J. Am. Chem. Soc.*, 2013, **135**, 18126.
- 28 K. L. Hu, M. Kurmoo, Z. Wang and S. Gao, *Chem. Eur. J.*, 2009, **15**, 12050.



graphics for TOC  
64x41mm (600 x 600 DPI)